

# Observation of a Field-induced Quantum Spin Liquid in $\alpha$ -RuCl<sub>3</sub>

S.-H. Baek,<sup>1,\*</sup> S.-H. Do,<sup>2</sup> K.-Y. Choi,<sup>2,†</sup> Y. S. Kwon,<sup>3</sup> A.U.B. Wolter,<sup>1</sup> S. Nishimoto,<sup>1,4</sup> Jeroen van den Brink,<sup>1,4</sup> and B. Büchner<sup>1,4</sup>

<sup>1</sup>*IFW Dresden, Helmholtzstr. 20, 01069 Dresden, Germany*

<sup>2</sup>*Department of Physics, Chung-Ang University, Seoul 156-756, Republic of Korea*

<sup>3</sup>*Department of Emerging Materials Science, DGIST, Daegu 711-873, Republic of Korea*

<sup>4</sup>*Department of Physics, Technische Universität Dresden, 01062 Dresden, Germany*

(Dated: February 7, 2017)

Topological quantum spin liquids (QSLs) are states of matter with remarkable predicted properties – an ability to create and braid quasiparticles in certain topological QSLs equals the ability to perform topologically protected quantum computation. There are various mathematical models with topological QSL phases, but so far none has been physically realized. Here we show that  $\alpha$ -RuCl<sub>3</sub> exhibits a magnetic field-induced QSL ground-state. Nuclear Magnetic Resonance measurements reveal that for fields larger than  $\sim 10$  T a spin-gap opens up while resonance lines remain sharp, evidencing that spins are quantum disordered. Such a field-induced, gapped topological QSL phase has been predicted in the Kitaev model, which is closely associated to  $\alpha$ -RuCl<sub>3</sub>. The quasiparticles in this phase of the Kitaev model have the statistical properties required for universal topological quantum computation.

When the interactions between magnetic spins are strongly frustrated, quantum fluctuations can cause spins to remain disordered even at very low temperatures [1]. The quantum spin liquid (QSL) state that ensues is conceptually very interesting – for instance new fractionalized excitations appear that are very different from the ordinary spin-wave excitations in ordered magnets [2–5]. A fascinating aspect of these quasiparticles is that not only their quantum numbers are fractions of those of the constituent spins, but that even their quantum *statistics* can be different. Specifically in *topological* QSLs quasiparticles can emerge that are neither bosons nor fermions – their statistics can be anywhere in between Bose and Fermi statistics and they are aptly named anyons [6, 7]. Topological quantum computing is conceptually based on the manipulation and braiding of such anyons, in particular anyons of the non-Abelian type. Such non-Abelian anyons appear in the so-called Kitaev honeycomb model in an external magnetic field – a prototypical and mathematically well-understood model of strongly frustrated interacting spins [8, 9].

This observation has motivated the search for the experimental realization of the Kitaev honeycomb model and its topological QSL phases. The quest was centered until recently mainly on honeycomb iridate materials [10, 11] of the type A<sub>2</sub>IrO<sub>3</sub>, where A = Na or Li. However, in these iridates long-range magnetic order develops at low temperatures for all known different crystallographic phases [12–16]. Their QSL regime is most likely preempted by the presence of significant residual Heisenberg-type interactions, by longer-range interactions between the spins or by crystallographically distinct Ir-Ir bonds, if not a combination of these factors [17–20]. More promising in this respect is ruthenium trichloride  $\alpha$ -RuCl<sub>3</sub> in its honeycomb crystal phase [21–28]. Neutron scattering studies have shown that the

magnetic interactions in this material are closer to the Kitaev limit [29]. But in spite of its proximity to QSL ground-state, at low temperatures and in zero magnetic field also this quasi-2D material exhibits long-range magnetic order.

It is well-known that the Kitaev model Hamiltonian harbors a topological QSL state not only for zero magnetic field – at which an Abelian QSL forms – but also at finite magnetic field, in which a non-Abelian QSL is stable [8, 9, 30]. In this Letter, we show by means of nuclear magnetic resonance (NMR) that in  $\alpha$ -RuCl<sub>3</sub> large external magnetic fields larger than  $\sim 10$  T melt the magnetic order and a spin-gap opens that scales linearly with magnetic field. At the same time the resonance lines remain very sharp, evidencing that the spins are quantum disordered and locally fluctuating. The state that emerges therefore exhibits all NMR signatures of a QSL showing that the detrimental effects of residual magnetic interactions between the Ru moments can be overcome by an external magnetic field that stabilizes a QSL state.

<sup>35</sup>Cl (nuclear spin  $I = 3/2$ ) NMR was carried out in a  $\alpha$ -RuCl<sub>3</sub> single crystal ( $2 \times 1 \times 0.5$  mm<sup>3</sup>) at an external field ( $H$ ) of 15 T and in the range of temperature ( $T$ ) 4.2 – 280 K. (See Supplementary Material (SM) for the crystal growth and characterization.) The sample was reoriented using a goniometer for the accurate alignment along  $\mathbf{H}$ . The <sup>35</sup>Cl NMR spectra were acquired by a standard spin-echo technique with a typical  $\pi/2$  pulse length 2–3  $\mu$ s. The nuclear spin-lattice relaxation rate  $T_1^{-1}$  was obtained by fitting the recovery of the nuclear magnetization  $M(t)$  after a saturating pulse to following fitting function,  $1 - M(t)/M(\infty) = A[0.9e^{-(6t/T_1)^\beta} + 0.1e^{-(t/T_1)^\beta}]$ , where  $A$  is a fitting parameter and  $\beta$  is the stretching exponent.

Experimentally in  $\alpha$ -RuCl<sub>3</sub> a very peculiar, strongly anisotropic magnetism has been reported previously [25–

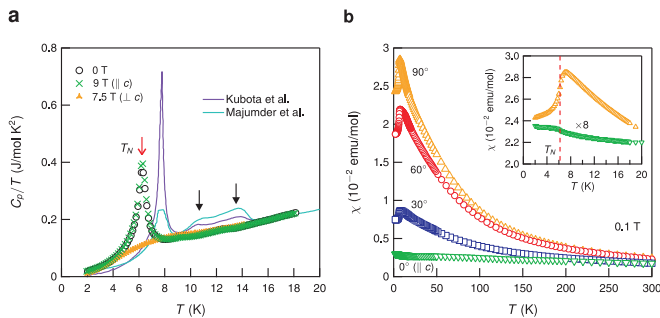


FIG. 1. **a**, Low- $T$  specific heat  $C_p/T$  at zero and chosen magnetic fields. The data at zero field taken from Refs. [27] and [26] are compared. **b**, Temperature dependence of the uniform magnetic susceptibility  $\chi$  at  $H = 0.1$  T obtained for the four different field orientations with respect to the  $c$  axis. The inset enlarges the low- $T$  region.

27] based on measurements of the uniform magnetic susceptibility  $\chi$  and the specific heat  $C_p/T$ . From the data it is clear that the antiferromagnetic (AFM) state observed at low  $T$  is hardly affected by external fields along the  $c$  direction whereas the signatures of the long range magnetic order seen in  $C_p/T$  and  $\chi(T)$  disappear for moderate fields of about 8 T applied along the  $ab$  plane. This pronounced anisotropy of the magnetism is also found in our crystals (see Fig. 1a and b). Note that whereas earlier studies [26, 27, 31] reported either two magnetic phase transitions at  $T_{N1} \sim 8$  K and  $T_{N2} \sim 14$  K or a single transition at  $T_N \sim 13$  K, our measurements of the magnetization and the specific heat show essentially a single transition occurring at a considerably lower temperature,  $T_{N1} \sim 6.2$  K. This evidences that our single crystal is of high quality with a (nearly) uniform stacking pattern [29, 32].

We now turn to the  $^{35}\text{Cl}$  NMR measurements on  $\alpha$ - $\text{RuCl}_3$ . Since the  $^{35}\text{Cl}$  nuclei possess a large quadrupole moment, the NMR spectra are strongly affected by the quadrupolar interaction determined by the electric field gradient (EFG). In  $\alpha$ - $\text{RuCl}_3$ , the principal axis of the largest eigenvalue of the EFG tensor  $V_{zz}$  at  $^{35}\text{Cl}$  is expected to point along the shared edges of the  $\text{RuCl}_6$  octahedra which are tilted  $\sim 35^\circ$  away from the  $c$  axis as illustrated in Fig. 2a.

As a result, there exist three inequivalent  $^{35}\text{Cl}$  sites, yielding a very complex and broad  $^{35}\text{Cl}$  spectrum in a magnetic field, as shown in Fig. 2b, which would make further NMR studies extremely difficult. However, taking advantage of the fact that the influence of the quadrupole interaction is very sensitive to the angle between the direction of  $V_{zz}$  and  $\mathbf{H}$ , it is possible to separate one  $^{35}\text{Cl}$  spectrum from other two spectra by applying  $H$  along one of the three directions of  $V_{zz}$  at  $^{35}\text{Cl}$ . Moreover, when  $\mathbf{H}$  is parallel to the direction of  $V_{zz}$ , the quadrupole line broadening should be significantly reduced, allowing further narrowing of the line.

Indeed, by rotating the sample in the  $ac$  plane, we achieved a very narrow single  $^{35}\text{Cl}$  line with the linewidth of 10 kHz at  $\theta \sim 30^\circ$  (see Fig. 2b). When the sample is reversely rotated by  $90^\circ$  (i.e.  $\mathbf{H}$  is perpendicular to the direction of  $V_{zz}$ ), we also detected a narrow  $^{35}\text{Cl}$  line. These observations confirm that  $V_{zz}$  is directed  $\sim 30^\circ$  from the  $c$  axis and it is convenient to present the NMR data for fields parallel and perpendicular to the direction of  $V_{zz}$ . We therefore define the direction of  $V_{zz}$  as the  $c'$  axis and in the following will present our NMR results with respect to the  $c'$  axis.

The  $T$ -dependence of the  $^{35}\text{Cl}$  NMR spectrum at 15 T are presented for  $H \parallel c'$  and  $H \perp c'$  in Fig. 2c. Clearly, there is no signature of long-range magnetic order, which would cause a large broadening or splitting of the  $^{35}\text{Cl}$  line. The absence of static magnetic order at 15 T  $\parallel c'$  is consistent with the disappearance of the specific heat anomaly above 9 T  $\parallel c'$  (see Fig. 4a). Another feature is the appearance of a new NMR peak that replaces the original peak below  $\sim 75$  K (see the inset of Fig. 2c). This is due to a first order structural phase transition, which is also inferred from the magnetic susceptibility [25, 27]; details are provided in the SM.

Figure 2d presents the  $T$  dependence of the resonance frequency  $\nu$  in terms of the NMR shift  $\mathcal{K} = (\nu - \nu_0)/\nu_0$  where  $\nu_0$  is the unshifted Larmor frequency.  $\mathcal{K}$  is composed, mainly, of the three terms:  $\mathcal{K} = A_{\text{hf}}\chi_{\text{spin}} + \mathcal{K}_{\text{chem}} + \mathcal{K}_{\text{quad}}$  where  $A_{\text{hf}}$  is the hyperfine (hf) coupling constant,  $\chi_{\text{spin}}$  the local spin susceptibility,  $\mathcal{K}_{\text{chem}}$  the  $T$  independent chemical shift, and  $\mathcal{K}_{\text{quad}}$  the second order quadrupole shift. Since  $\mathcal{K}_{\text{quad}}$  which is determined by the charge distribution around the  $^{35}\text{Cl}$  nucleus only weakly changes with  $T$ , the strong upturn of  $\mathcal{K}$  observed at low  $T$  has to be attributed to  $\chi_{\text{spin}}$  which is in good agreement with the macroscopic susceptibility (see Fig. 1c).

The most striking result of our NMR measurements is the  $H$  and  $T$  dependence of  $T_1^{-1}$ . Figure 2e shows the  $T$  dependence of  $T_1^{-1}$  at  $H = 15$  T oriented both parallel and perpendicular to  $c'$ . For the discussion of these data we divide the temperature range in three parts. At high  $T$  above  $T^* \sim 160$  K,  $T_1^{-1}$  follows roughly the behavior expected for simple paramagnets;  $T_1^{-1}$  is nearly independent of  $T$ . The different absolute values of  $T_1^{-1}$  for the two orientation of  $H$  are ascribed to the anisotropic hf couplings which are expected in this highly two-dimensional layered material. Indeed, the comparison of the NMR shift and the magnetic susceptibility gives rise to the sizable anisotropy of the hf couplings, see the inset of Fig. 2d and the SM for detailed discussion.

As  $T$  is lowered below  $T^*$ ,  $T_1^{-1}$  increases for  $H \parallel c'$  but it decreases for  $H \perp c'$ . Since the spin-lattice relaxation process is induced by the transverse components of spin fluctuations (SFs) with respect to the nuclear quantization axis, it is clear that  $T_1^{-1}$  for  $H \parallel c'$  experiences stronger in-plane and weaker out-of-plane SFs than for

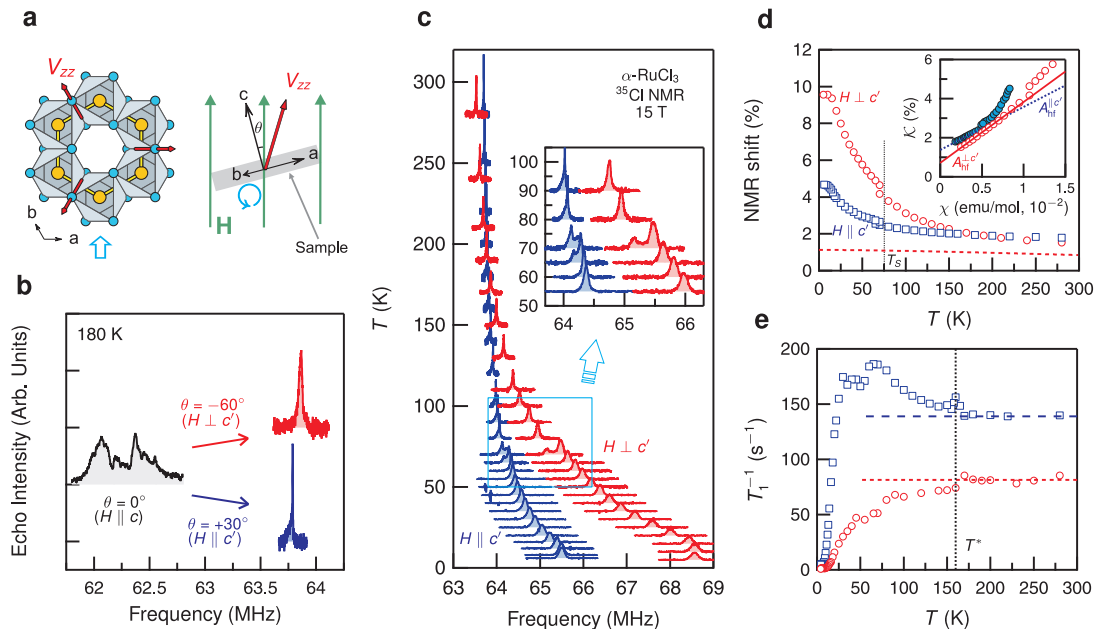


FIG. 2. **a**, The principal axis of the electric field gradient  $V_{zz}$  at the  $^{35}\text{Cl}$  nuclei is along the shared edges of the  $\text{RuCl}_6$  octahedra, resulting in three inequivalent  $^{35}\text{Cl}$  sites in field. The sample is mounted on the goniometer so that one of the three axes of  $V_{zz}$ 's lies in the rotating plane. **b**, When  $H \parallel c$  ( $\theta = 0$ ), the  $^{35}\text{Cl}$  spectrum is extremely complex and broad. As  $H$  is either parallel or perpendicular to the direction of  $V_{zz}$ , very narrow  $^{35}\text{Cl}$  NMR lines were obtained. **c**,  $^{35}\text{Cl}$  NMR spectrum measured at  $H = 15$  T as a function of  $T$  with cooling for two different field orientations. The first order character of the structural transition is evidenced by the gradual transfer of the  $^{35}\text{Cl}$  spectral weight below  $T_S \sim 75$  K, as clearly shown in the inset. **d**, NMR shift  $\mathcal{K}$  as a function of  $T$ . The strong anisotropy of  $\mathcal{K}$  increases rapidly with decreasing  $T$ , approaching a saturated value below  $\sim 10$  K. The dotted line is the estimated  $T$  dependence of  $\mathcal{K}_{\text{quad}}$  (see the SM for details). The inset shows the  $\mathcal{K}$  vs  $\chi$  plot, which yields the hyperfine coupling constants,  $A_{\text{hf}}^{\perp c'} = 17.4$  kG/ $\mu_B$  and  $A_{\text{hf}}^{\parallel c'} = 12.3$  kG/ $\mu_B$ . **e**, Spin-lattice relaxation rate  $T_1^{-1}$  as a function of  $T$ . Whereas  $T_1^{-1}$  is nearly  $T$ -independent above  $T^* = 160$  K, it increases (decreases) for  $H \parallel c'$  ( $H \perp c'$ ) below  $T^*$ , implying the development of in-plane spin correlations.

$H \perp c'$ . Hence, the increase of the  $T_1^{-1}$  anisotropy with lowering  $T$  is an indication of the development of strong in-plane SFs below  $T^*$ . Remarkably, we find a small but discernible anomaly at  $T^*$  for both field orientations. Thus  $T^*$  is straightforwardly related to the development of magnetic correlations upon cooling.

In the low  $T$  region, roughly below 50 K,  $T_1^{-1}$  starts to decrease similarly for both field directions. For the study of spin dynamics at low  $T$ , it is convenient to consider the quantity  $(T_1 T)^{-1}$ , which is proportional to the  $\mathbf{q}$ -average of the imaginary part of the dynamical susceptibility,  $\sum_{\mathbf{q}} A_{\text{hf}}^2(\mathbf{q}) \chi''(\mathbf{q}, \omega_0) / \omega_0$ , where  $\omega_0$  is the Larmor resonance frequency, probing low-energy spin excitations. The  $T$  dependence of  $(T_1 T)^{-1}$  is shown in Fig. 3a. A broad maximum of  $(T_1 T)^{-1}$  occurs near 30 K, being followed by a rapid drop towards low  $T$  in an identical manner for both field orientations. The rapid decrease of  $(T_1 T)^{-1}$  implies a pronounced depletion of spectral weight in the spin excitation spectrum at low  $T$ . The semilog plot of  $T_1^{-1}$  against  $1/T$  drawn in Fig. 3b unambiguously reveals a spin gap behavior, i.e.,  $T_1^{-1} \propto \exp(-\Delta/T)$ , with the activation energy  $\Delta \sim 44$  and 50 K for  $H \parallel c'$  and  $\perp c'$ , respectively.

An explanation of the observed spin-gap in terms of static magnetic order can be ruled out. For example, the  $^{35}\text{Cl}$  spectra measured at  $H = 15$  T do not show any signature of magnetic order down to 4.2 K (see Fig. 2c), in agreement with the conclusions from specific heat and magnetization. Moreover, it is difficult to attribute the extracted large spin gap to some kind of anisotropy gap occurring in the spin wave spectrum in magnetically ordered systems. As displayed in Fig. 3a, the low temperature behavior of the spin-lattice relaxation is very similar for both field orientations, indicating that spin dynamics is nearly isotropic at least in the range of field orientations ( $30^\circ - 60^\circ$  off the  $ab$  plane). Therefore, not only the measured large gap size but also the isotropic gap behavior contradict any interpretation in terms of anisotropy gaps. The findings are in particular not compatible with the gap being due to a saturating ferromagnetic polarization of spins. While the values of magnetisation and Knight shift strongly depend on the field orientation, the spin gap does not. In other words, a gap of similar size is observed for spins close to the AFM alignment ( $H \perp$  to the planes) and for the perpendicular direction showing a much larger magnetisation, which rules out any dis-

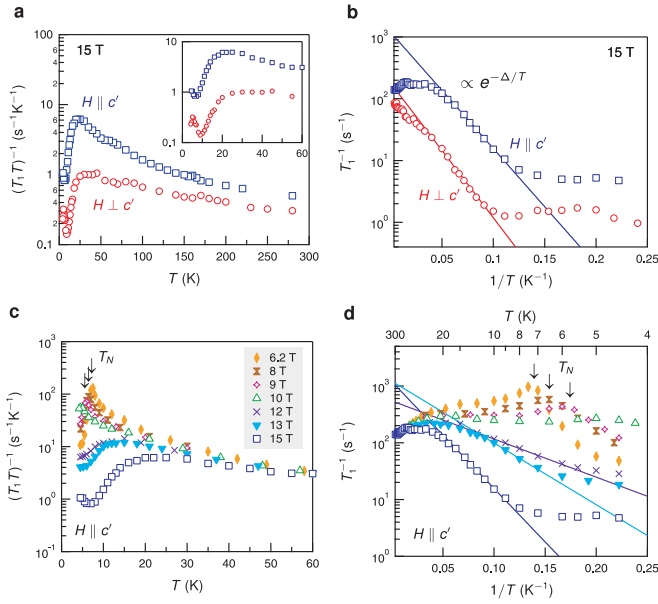


FIG. 3. **a**,  $(T_1T)^{-1}$  as a function of  $T$  measured at 15 T. At low  $T$ ,  $(T_1T)^{-1}$  for both field directions reaches a maximum at  $\sim 25$  K which is followed by a rapid drop upon further cooling. Inset enlarges the low  $T$  region. **b**, Semilog plot of  $T_1^{-1}$  vs.  $1/T$  unravels a spin gap behavior  $T_1^{-1} \propto \exp(-\Delta/T)$ . The deviation from the gap behavior takes place below  $\sim 10$  K. **c**, Strong field dependence of  $(T_1T)^{-1}$  at low  $T$  as a function of  $H \parallel c'$ . Below 9 T, AFM ordered phase was clearly detected by sharp peaks of  $(T_1T)^{-1}$ . **d**, The spin gap  $\Delta$  is rapidly filled up with decreasing  $H \parallel c'$ , vanishing completely at 10 T.

discussion of our data in terms of ferromagnetic polarized spins. This clear-cut conclusion from the bare experimental findings is further supported by a detailed theoretical analysis. Calculating the spin-flip spectrum by Lanczos exact cluster diagonalization (see SM) shows that the experimentally observed magnitude and on-set field of the gap are incompatible with it being due to field-forced ferromagnetism.

In order to study the  $H$  dependence of the spin gap, we measured  $T_1^{-1}$  as a function of  $H \parallel c'$  in the low  $T$  region. The results are shown in Fig. 3c and 3d. A spin gap is only seen for  $H > 10$  T. In this field range  $\Delta$  increases with increasing  $H$ . At  $H = 10$  T our data show a Curie like upturn of the SFs, i.e.  $(T_1T)^{-1}$  diverges for low  $T$ . Upon further lowering  $H$  below 10 T, a sharp peaks in  $(T_1T)^{-1}$  signals static magnetic order below a characteristic temperature  $T_N$  which decreases with increasing  $H$ . In the magnetically ordered phase, the  $^{35}\text{Cl}$  spectrum progressively spreads out with decreasing  $T$ , indicating the incommensurate character of AFM order [26], see Fig. S3 in the SM for the spectrum in the ordered state. Thus, our data for  $(T_1T)^{-1}$  clearly show a qualitative change of the behavior as a function of  $H$ : the peak due to static order occurring at low field is replaced by a spin gap like behavior at  $H \geq 10$  T. At the bor-

der the spin dynamics suggests quantum criticality, i.e. a divergence of  $(T_1T)^{-1}$  for  $T = 0$ .

To back our NMR findings, we measured the specific heat  $C_p/T$  for  $H \parallel c'$ , as shown in Fig. 4a. The specific heat anomaly associated with AFM order is rapidly suppressed toward 10 T, which perfectly agrees with the  $T_1^{-1}$  results shown in Fig. 3c-d. Further, we confirmed that at 14 T  $C_p/T$  is significantly suppressed in the low  $T$  region, evidencing the opening of a spin gap at  $H > 10$  T. Quantitative analysis of the gap from specific heat data at low  $T$  is difficult, partially due to uncertainties of the phonon background. Modelling this background on the basis of the data of non-magnetic isostructural  $\text{RhCl}_3$  and assuming a simple exponential law yields a value of  $\Delta \sim 20$  K at 13.9 T (see the SM) in rough agreement with the NMR findings.

The data thus indicate a field induced crossover from a magnetically ordered state at low fields to a disordered state showing gapped spin excitations in large fields. As evident from Fig. 3d,  $T_1^{-1}$  deviates from the gap behavior at very low  $T$  and becomes almost  $T$  independent. This suggests short-range SFs coexisting with the spin-gap in the high field phase. A very clear-cut behavior is found at higher temperatures  $T \geq 10$  K. Here  $T_1^{-1}$  changes systematically with increasing  $H$ , yielding the spin gap  $\Delta$  that increases linearly with  $H$ .

It is interesting to note that for the pure Kitaev model a magnetic field generates in lowest order perturbation theory an excitation gap proportional to the field cubed [8]. In  $\alpha\text{-RuCl}_3$  certainly magnetic interactions beyond the pure Kitaev exchange are of relevance [23, 25, 29, 33] – how the perturbation results for the pure model are affected by the significant residual interactions in presence of a magnetic field is at the moment an open theoretical question. Extrapolating the curve to lower fields yields a threshold value of  $H_c \sim 10$  T, i.e. the same field where the  $T$  dependence of the  $T_1^{-1}$  changes its qualitative behavior from an upturn to a downturn at low  $T$ . Fig. 3d also shows a low  $T$  flattening out of  $T_1^{-1}$  indicating the presence of another very low energy scale for spin dynamics. This feature is likely related to inhomogeneous states for instance due to magnetic defects. Its becoming suppressed with increasing  $H$  is consistent with competition between partially defect induced magnetism and a spin gap that increases with  $H$ . We find in conclusion that a magnetic field induces the suppression of slow magnetic fluctuations as well as the increase of  $\Delta$  in the high field region. These point to the same critical field separating a magnetically ordered state from a disordered state exhibiting a large magnetic field dependent spin gap.

Our NMR findings of  $T_N$  and  $\Delta$  as a function of  $H$  are summarized in the  $H$ - $T$  phase diagram shown in Fig. 4b. Note that the suppression of AFM order for  $H \parallel c'$  occurs at  $\sim 10$  T, which is only slightly higher than  $\sim 9$  T observed for  $H \parallel ab$ . This observation is striking because for  $H \parallel c'$  the field strength projected to the honeycomb

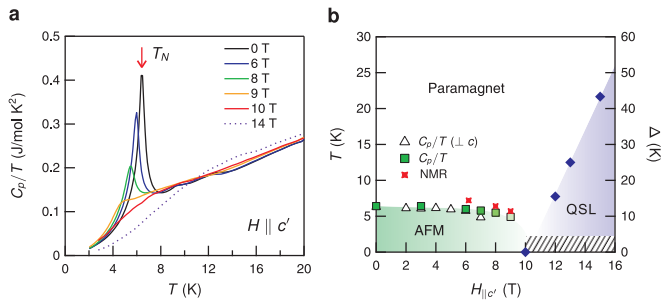


FIG. 4. **a**, The dependence of  $C_p/T$  on  $H$  oriented along  $c'$  ( $30^\circ$  off the  $c$  axis). With increasing  $H$ , magnetic order is suppressed and completely disappears at 10 T - at 14 T a gap appears to be present. **b**, The  $T$ - $H$  phase diagram obtained by NMR and specific heat measurements.  $T_N$  obtained by specific heat for  $H \perp c$  (empty triangle) is compared. The very low temperature phase for  $H > 10$  T, marked in the shaded area, is governed by inhomogeneous states for instance related to magnetic defects. In the QSL region of the phase diagram the measured field dependence of the spin-gap  $\Delta$  is shown (right axis).

plane is only half the applied one. This suggests that the AFM order is robust only when  $H$  is nearly parallel to the normal direction of the plane.

Previously it was established on theoretical and experimental grounds that the magnetic interactions between the quantum spins in  $\alpha$ - $\text{RuCl}_3$  are well-described by the Kitaev model, however in the presence of residual interactions which ultimately preempt the QSL state in zero magnetic field [21–27, 29, 34]. In the pure Kitaev model at zero-field, the ground-state is an Abelian QSL that is gap-less [8] and the present observations suggest that the absence of a gap leaves this Abelian QSL very susceptible to the perturbing residual interactions that drive the formation of long-range magnetic order. In finite field, however, a non-Abelian QSL forms in the pure honeycomb Kitaev model, which is protected by a spin gap [8]. The data suggest that when the external magnetic field and gap become large enough it can overcome the energy scale related to the residual magnetic interactions so that a QSL emerges.

This work has been supported by the Deutsche Forschungsgemeinschaft (Germany) via DFG Research Grants BA 4927/1-3 and the collaborative research center SFB 1143. JvdB acknowledges support from the Harvard-MIT CUA.

[1] L. Balents, *Nature* **464**, 199 (2010).  
 [2] Y. Shimizu, K. Miyagawa, K. Kanoda, M. Maesato, and G. Saito, *Phys. Rev. Lett.* **91**, 107001 (2003).  
 [3] M. Yamashita, N. Nakata, Y. Senshu, M. Nagata, H. M. Yamamoto, R. Kato, T. Shibauchi, and Y. Matsuda, *Science* **328**, 1246 (2010).

[4] T.-H. Han, J. S. Helton, S. Chu, D. G. Nocera, J. A. Rodriguez-Rivera, C. Broholm, and Y. S. Lee, *Nature* **492**, 406 (2012).  
 [5] M. Fu, T. Imai, T.-H. Han, and Y. S. Lee, *Science* **350**, 655 (2015).  
 [6] J. M. Leinaas and J. Myrheim, *Il Nuovo Cimento B* **37**, 1 (1977).  
 [7] F. Wilczek, *Phys. Rev. Lett.* **49**, 957 (1982).  
 [8] A. Kitaev, *Annals of Physics* **321**, 2 (2006).  
 [9] J. K. Pachos, *Introduction to Topological Quantum Computation* (Cambridge University Press, Cambridge, UK, 2012).  
 [10] G. Jackeli and G. Khaliullin, *Phys. Rev. Lett.* **102**, 017205 (2009).  
 [11] J. Chaloupka, G. Jackeli, and G. Khaliullin, *Phys. Rev. Lett.* **105**, 027204 (2010).  
 [12] Y. Singh and P. Gegenwart, *Phys. Rev. B* **82**, 064412 (2010).  
 [13] F. Ye, S. Chi, H. Cao, B. C. Chakoumakos, J. A. Fernandez-Baca, R. Custelcean, T. F. Qi, O. B. Korneta, and G. Cao, *Phys. Rev. B* **85**, 180403 (2012).  
 [14] S. K. Choi, R. Coldea, A. N. Kolmogorov, T. Lancaster, I. I. Mazin, S. J. Blundell, P. G. Radaelli, Y. Singh, P. Gegenwart, K. R. Choi, S.-W. Cheong, P. J. Baker, C. Stock, and J. Taylor, *Phys. Rev. Lett.* **108**, 127204 (2012).  
 [15] T. Takayama, A. Kato, R. Dinnebier, J. Nuss, H. Kono, L. Veiga, G. Fabbris, D. Haskel, and H. Takagi, *Phys. Rev. Lett.* **114**, 077202 (2015).  
 [16] K. A. Modic, T. E. Smidt, I. Kimchi, N. P. Breznay, A. Biffin, S. Choi, R. D. Johnson, R. Coldea, P. Watkins-Curry, G. T. McCandless, J. Y. Chan, F. Gandara, Z. Islam, A. Vishwanath, A. Shekhter, R. D. McDonald, and J. G. Analytis, *Nature Communications* **5**, 4203 (2014).  
 [17] I. Kimchi and Y.-Z. You, *Phys. Rev. B* **84**, 180407 (2011).  
 [18] J. G. Rau, E. K.-H. Lee, and H.-Y. Kee, *Phys. Rev. Lett.* **112**, 077204 (2014).  
 [19] V. M. Katukuri, S. Nishimoto, V. Yushankhai, A. Stoyanova, H. Kandpal, S. Choi, R. Coldea, I. Rousochatzakis, L. Hozoi, and J. van den Brink, *New Journal of Physics* **16**, 013056 (2014).  
 [20] S. Nishimoto, V. M. Katukuri, V. Yushankhai, H. Stoll, U. K. Rößler, L. Hozoi, I. Rousochatzakis, and J. van den Brink, *Nature Communications* **7**, 10273 (2016).  
 [21] K. W. Plumb, J. P. Clancy, L. J. Sandilands, V. V. Shankar, Y. F. Hu, K. S. Burch, H.-Y. Kee, and Y.-J. Kim, *Phys. Rev. B* **90**, 041112 (2014).  
 [22] I. Rousochatzakis, J. Reuther, R. Thomale, S. Rachel, and N. B. Perkins, *Phys. Rev. X* **5**, 041035 (2015).  
 [23] H.-S. Kim, V. S. Shankar V., A. Catuneanu, and H.-Y. Kee, *Phys. Rev. B* **91**, 241110 (2015).  
 [24] L. J. Sandilands, Y. Tian, A. A. Reijnders, H.-S. Kim, K. W. Plumb, Y.-J. Kim, H.-Y. Kee, and K. S. Burch, *Phys. Rev. B* **93**, 075144 (2016).  
 [25] J. A. Sears, M. Songvilay, K. W. Plumb, J. P. Clancy, Y. Qiu, Y. Zhao, D. Parshall, and Y.-J. Kim, *Phys. Rev. B* **91**, 144420 (2015).  
 [26] M. Majumder, M. Schmidt, H. Rosner, A. A. Tsirlin, H. Yasuoka, and M. Baenitz, *Phys. Rev. B* **91**, 180401 (2015).  
 [27] Y. Kubota, H. Tanaka, T. Ono, Y. Narumi, and K. Kindo, *Phys. Rev. B* **91**, 094422 (2015).  
 [28] J. Nasu, J. Knolle, D. L. Kovrizhin, Y. Motome, and

- R. Moessner, *Nature Physics* **12**, 912 (2016).
- [29] A. Banerjee, C. A. Bridges, J.-Q. Yan, A. A. Aczel, L. Li, M. B. Stone, G. E. Granroth, M. D. Lumsden, Y. Yiu, J. Knolle, S. Bhattacharjee, D. L. Kovrizhin, R. Moessner, D. A. Tennant, D. G. Mandrus, and S. E. Nagler, *Nature Mater.* **15**, 733 (2016).
- [30] Z. Nussinov and J. van den Brink, *Rev. Mod. Phys.* **87**, 1 (2015).
- [31] R. D. Johnson, S. C. Williams, A. A. Haghighirad, J. Singleton, V. Zapf, P. Manuel, I. I. Mazin, Y. Li, H. O. Jeschke, R. Valentí, and R. Coldea, *Phys. Rev. B* **92**, 235119 (2015).
- [32] H. B. Cao, A. Banerjee, J.-Q. Yan, C. A. Bridges, M. D. Lumsden, D. G. Mandrus, D. A. Tennant, B. C. Chakoumakos, and S. E. Nagler, *Phys. Rev. B* **93**, 134423 (2016).
- [33] R. Yadav, N. A. Bogdanov, V. M. Katukuri, S. Nishimoto, J. van den Brink, and L. Hozoi, *Sci. Rep.* **6**, 37925 (2016).
- [34] L. J. Sandilands, Y. Tian, K. W. Plumb, Y.-J. Kim, and K. S. Burch, *Phys. Rev. Lett.* **114**, 147201 (2015)

## Supplementary Materials to “Observation of a Field-induced Quantum Spin Liquid in $\alpha$ -RuCl<sub>3</sub>”

### Crystal growth and characterization

High quality single crystals of  $\alpha$ -RuCl<sub>3</sub> were grown by a vacuum sublimation method. A commercial RuCl<sub>3</sub> powder (Alfa-Aesar) was thoroughly ground, and dehydrated in a quartz ampoule at 250°C for two days. The ampoule was sealed in vacuum and placed in a temperature gradient furnace. The temperature of the RuCl<sub>3</sub> powder was set at 1080°C. After five hours the furnace was cooled to 600°C at a rate of -2°C/h. The obtained crystals were black and have wide shiny surfaces of  $3 \times 3$  mm<sup>2</sup>. The surfaces are parallel to the  $ab$  plane and are easily cleaved. Their magnetic properties were investigated using a commercial SQUID magnetometer (Quantum Design, MPMS-5XL). Specific-heat measurements of the single crystals ( $3 \times 3 \times 1$  mm<sup>3</sup>, and  $m \approx 20$  mg) were performed using commercial Quantum Design platforms (PPMS calorimeter).

### Magnetic susceptibility

The temperature dependence of the magnetic susceptibility  $\chi(T)$  is presented in Fig. 1c of the main text. Depending on the orientation of the magnetic field the temperature dependence of  $\chi(T)$  shows qualitatively different behavior and an analysis in terms of a Curie-Weiss law reveals Curie-Weiss temperatures with different signs. While  $\chi(T)$  remains very small for fields parallel to the  $c$  axis, it strongly diverges at low  $T$  for  $H \parallel ab$  suggesting ferromagnetic interactions. Here we expound the peculiar magnetic properties of  $\chi(T)$ . As evident from the temperature dependence of the inverse susceptibility plotted in Fig. S1a, for temperatures above 120 K  $\chi(T)$  follows the Curie-Weiss law. The low-temperature deviation of  $\chi(T)$  from the Curie-Weiss law means that short-range magnetic correlations persist to temperatures on the order of 120 K. Noteworthy is that a nearly  $T$ -independent magnetic Raman response was observed below 100 – 120 K and was attributed to the system being in the vicinity of a spin-liquid phase [1]. In addition, the temperature dependence of the spin-lattice relaxation rate,  $T_1^{-1}$ , shows a signature of developing in-plane spin correlations at  $T^* = 160$  K (see Fig. 2e of the main text).

The Curie-Weiss fit of  $\chi(T)$  in the range of 120 K to room temperature gives a Curie-Weiss temperature of  $\Theta_{CW} = -270$  K for  $H \parallel c$  and 33 K for  $H \parallel ab$ . The very large frustration parameter of  $|\Theta_{CW}/T_N| = 42$  lends support to the system being in the proximity of a spin liquid state. The anisotropy of  $\Theta_{CW}$  suggests that the easy axis is perpendicular to the  $c$  axis. According to the high temperature expansion formula for the extended

Kitaev-Heisenberg system[2], the anisotropy of  $\Theta_{CW}$  is given by  $(\Theta_c - \Theta_{ab})/(\Theta_c + 2\Theta_{ab}) = \Gamma/(3J + K) \sim 3/2$ . Assuming the values of  $J = -2.9$  meV and  $K = 8.1$  meV from inelastic neutron scattering measurements[29], we obtain  $\Gamma = -0.9$  meV. This set of the magnetic parameters determines the  $\Gamma - J - K$  phase diagram. The effective moment of  $\mu_{\text{eff}} = 2.72 \mu_B$  obtained from the  $H \parallel c$  data is larger than  $\mu_{\text{eff}} = 2.25 \mu_B$  from the  $H \parallel ab$  one. Noticeably, these values are much larger than the spin only value of  $1.73\mu_B$  expected for Ru<sup>3+</sup> ( $S = 1/2$ ), substantiating a large orbital contribution to the magnetic moment.

In addition to the magnetic anomaly, at high temperatures  $\chi(T)$  displays a distinct jump and pronounced hysteresis in the warming and cooling process as shown in the inset of Fig. S1a. This is ascribed to the first-order structural phase transition[3] from  $C2/m$  to  $R-3$ . From the fact that the high- $T$  anomaly is observed only in the out-of-plane direction, we infer that interlayer interactions are largely affected by the structural transition while the intralayer interactions remain intact. Further, we note that the structure related anomaly in  $\chi(T)$  is hardly visible in other samples. This may be due to substantial stacking disorders and points at a high quality of our crystals.

Figure S1c presents the field dependence of  $\chi(T)$  in the low temperature range of  $T = 2 - 25$  K for  $H \perp c$ . At  $H = 0.1$  T  $\chi(T)$  exhibits a sharp maximum at around 8 K with decreasing temperature, being in agreement with the earlier reports [3–5]. From the derivative of  $\chi(T)$  shown in the inset of Fig. S1c, we identify a magnetic transition at  $T_N = 6.2$  K, but we cannot see any clear anomaly at 14 K. Compared to the earlier works [3–5], the transition temperature is lower by a few Kelvins. Applying an external field, the maximum position and  $T_N$  shift to lower temperature. The resulting field dependence of  $T_N$  is plotted in Fig. S2d (open triangles).

Figure S1d displays the magnetization vs field measured at 2 K for  $H \perp c$  and  $H \parallel c$ . The anisotropic magnetization curve  $M(B)$  confirms that the magnetic easy axis is in the  $ab$  plane. Indeed, an anticipated spin-flop transition is discernible at  $H_{\text{SF}} = 0.9$  T from the derivative  $dM(B)/dB$  (solid line) when an external field is applied along an easy axis. Apart from the spin-flop transition, we observe another magnetization jump at  $H = 5.8$  T. It is striking that the metamagnetic transition field of 5.8 T is comparable to an energy scale of  $T_N$ . As discussed in the main text and below, this metamagnetic transition corresponds to a field-induced quantum phase transition to a quantum disordered phase.

### Specific heat

Figure S2 summarizes the temperature dependence of specific heat  $C_p/T$  for the three  $\alpha$ -RuCl<sub>3</sub> samples taken

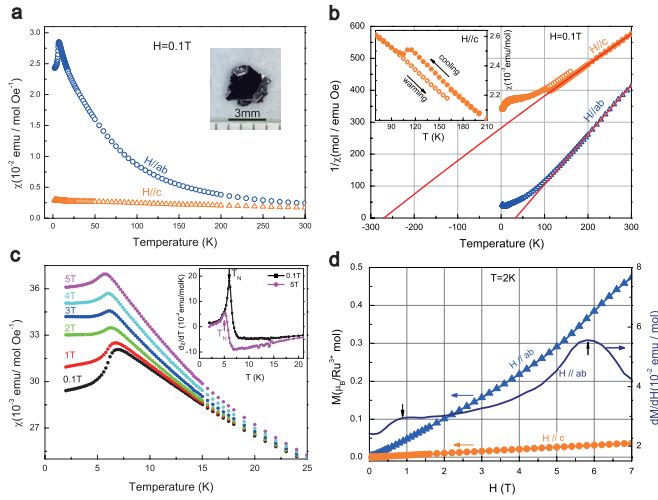


FIG. S1. **a**, Temperature dependence of magnetic susceptibility measured at  $H = 0.1$  T for a field parallel and perpendicular to the honeycomb  $ab$  plane. The inset shows a photograph of the single crystal used for experiments. **b**, Temperature dependence of inverse magnetic susceptibility for  $H \perp c$  and  $H \parallel c$  measured at  $H = 0.1$  T. The black lines are fits to the Curie-Weiss law. The inset shows a jump and hysteresis in the magnetic susceptibility associated with a first-order structural transition. **c**, Field and temperature dependence of the magnetic susceptibility measured in the field range of 0.1 – 5 T for  $H \perp c$ . The inset shows a derivative of the magnetic susceptibility, identifying a magnetic transition temperature at  $H = 0.1$  and 5 T. **d**, Magnetization vs field measured at  $T = 2$  K for  $H \perp c$  and  $H \parallel c$  together with its field derivative for  $H \perp c$ . The vertical arrows indicate a spin-flop-like transition at 0.9 T and a metamagnetic transition at 5.8 T.

at different batches, named sample #1, sample #2, and sample #3. For all samples,  $C_p/T$  shows a  $\lambda$ -like anomaly at 6.2 K, further confirming the long-range magnetic order. Our data revealed a strain-induced enhancement of the 13 K transition as shown in panel a. This result is related to a recent neutron diffraction finding[6] where the 13 K transition is linked to the ABAB-type stacking fault while the 6 K transition is associated with the ABCABC-type stacked honeycomb lattice. The mechanical deformation gains prosperity of the ABAB stacking fault, compared to the unstrained sample #3. As the long-range magnetic ordering temperature is determined by an interlayer interaction, this in turn strengthens the 13 K anomaly. In the process of sample preparation for specific heat measurements, a mechanical strain was inevitably exerted on samples while cutting and pressing the crystals for a good thermal contact between the sample and calorimeter platform. This strain effect becomes strong for  $H \perp c$  due to the large contact area as demonstrated in panel b.

With increasing field above 7.5 T the peaks of  $C_p/T$  at zero field turn into a weak hump, evidencing the development of short-range spin correlations while suppressing

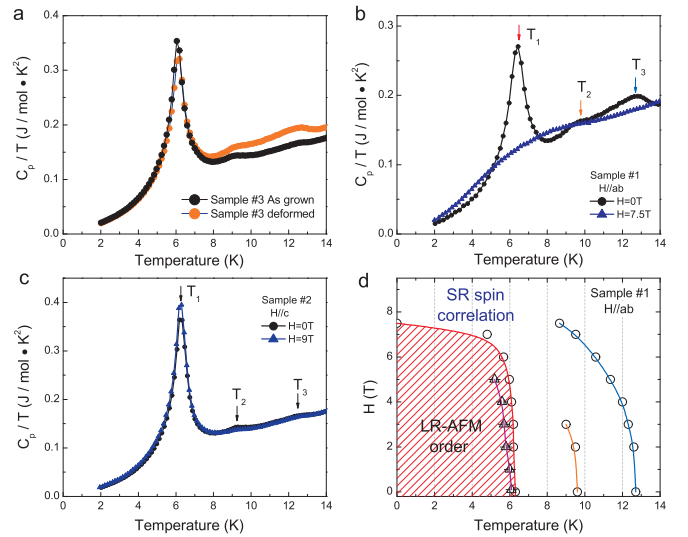


FIG. S2. **a**, Comparison of low-temperature specific heat  $C_p/T$  between as-grown and mechanically strained sample #3. **b**, Comparison of  $C_p/T$  of sample #1 between  $H = 0$  and 7.5 T for  $H \parallel ab$ . The vertical arrows indicate the magnetic anomalies. The magnetic orders are strongly suppressed at  $H = 7.5$  T. **c**, Comparison of  $C_p/T$  of sample #2 between  $H = 0$  and 9 T for  $H \parallel c$ . The magnetic transitions hardly vary with field. **d**, Field vs temperature phase diagram of sample #1 for  $H \parallel ab$ . The open circle symbols are the transition temperatures determined from the specific heat data and the open triangle symbols are ones from the magnetic susceptibility.

the long-range magnetic order. We note that the magnetic entropy is not conserved at the high-field phase in the low-temperature range  $1.5 \text{ K} < T < 14 \text{ K}$  because only a small part of the expected total magnetic entropy is released at the corresponding temperatures. Much of entropy release will take place at temperatures higher than 14 K as the consequence of the thermal fractionalization of spins, representing a characteristic signature of a Kitaev model system. As plotted in panel c, there is no appreciable field dependence of  $C_p/T$  for  $H \parallel c$ . It is notable that mainly a single transition is visible because the strain is minimized in the sample preparation for this geometry. Since NMR is a contact-free technique, the investigated crystals can be assumed to have a nearly uniform stacking order.

In panel d, we summarize the field-temperature phase diagram drawn from the sample #3 for  $H \parallel ab$ . Applying an external field above 7.5 T,  $\alpha\text{-RuCl}_3$  undergoes a quantum phase transition from the long-range AFM order to the short-range correlated phase.

### Specific heat analysis at 13.9 T

The spin gap  $\Delta$  was estimated from the specific heat data measured at  $H_{\parallel c} = 13.9$  T. After subtracting the

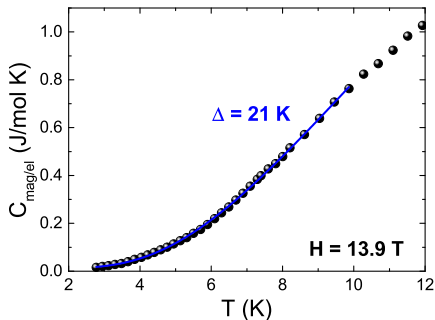


FIG. S3. The specific heat of  $\alpha$ -RuCl<sub>3</sub> subtracted by the phononic contribution in a magnetic field  $H_{\parallel c'} = 13.9$  T. The blue line represents a fit using a combined exponential activation law together with a linear (electronic) term for temperatures up to 10 K.

lattice contribution using the specific heat data obtained in the isostructural non-magnetic analogue RhCl<sub>3</sub>, the resulting specific heat  $C_{\text{mag/el}}$  was analyzed using the sum of an activation law and a linear term,

$$C_{\text{mag/el}} = A \exp(-\Delta/T) + \gamma T, \quad (1)$$

where  $A$  is the constant (see Fig. S3). The linear (electronic) term with a small  $\gamma$  is needed because the simple activation law failed to describe the data at  $T < 5$  K.

The fit of the data up to 10 K using the above formula yields  $\Delta = 21(2)$  K with a small  $\gamma = 5(2)$  mJ/mol K<sup>2</sup>. Although the obtained  $\Delta$  is a factor of two smaller than that determined by the NMR measurements, it unambiguously confirms the emergence of the spin gapped phase in the high magnetic fields above 10 T (See Fig. 4).

#### NMR peak below $\sim 75$ K

Below  $\sim 75$  K, we observed a new NMR peak that appears at a higher frequency and replaces the original low frequency peak with decreasing temperature, see the inset of Fig. 2c. This transfer of the <sup>35</sup>Cl spectral weight is attributed to the change of the EFG associated with a first order structural phase transition, which is also inferred from the magnetic susceptibility[4, 5] revealing a weak discontinuous change accompanied by a clear hysteresis when comparing measurements upon heating and cooling. It is interesting to note that  $T_S$  significantly differs when comparing the susceptibility and the NMR results. While  $\chi$  suggests  $T_S > 120$  K upon cooling, a much smaller transition temperature  $T_S \sim 75$  K is inferred from the NMR data. We attribute this difference to the well known “mechanical softness” of the compound which implies that cooling conditions, fixing of samples etc. strongly affects the samples. In order to avoid any

influence of the hysteretic behavior all data reported below have been measured upon cooling and stabilizing temperatures for a long time. The data show that the structural transition has no or only a minor influence on the magnetism of  $\alpha$ -RuCl<sub>3</sub> and for the present purposes can be disregarded.

#### Estimation of the second order quadrupole shift, $\mathcal{K}_{\text{quad}}$

Due to the presence of the three inequivalent <sup>35</sup>Cl sites in field, it is challenging to obtain the precise temperature dependence of the quadrupole frequency  $\nu_Q$  and the anisotropy parameter,  $\eta$ . Nevertheless, it is still possible to make an approximation of  $\nu_Q(T)$ . Assuming axial symmetry at the nuclei, the second order quadrupole shift is given by  $\Delta\nu(\theta) = 3\nu_Q^2/16\gamma_n H(1 - \cos^2\theta)(1 - 9\cos^2\theta)$  where  $\theta$  is the angle between the principal axis of the largest EFG,  $V_{zz}$ , and  $H$ . Since  $\mathcal{K}_{\text{quad}}$  disappears for  $\theta = 0$ , it is only important for  $H$  applied perpendicular to the axis of  $V_{zz}$ , i.e., for  $60^\circ$  off  $c$ . From the angle dependence of the <sup>35</sup>Cl spectra (see Fig. 2b), one can deduce that  $\Delta\nu(\pi/2) - \Delta\nu(\pi/6) \sim 1.5$  MHz, yielding  $\nu_Q \sim 14$  MHz at 180 K. Phenomenologically, a thermal contribution to the quadrupole frequency is described by  $\nu_Q(T) = \nu_Q^0 - aT^{3/2}$ , where  $\nu_Q^0$  is the value at  $T = 0$ . [7] A reasonable behavior of  $\mathcal{K}_{\text{quad}}$  is then estimated, which is shown as the dotted line in Fig. 2d, choosing  $a = 4 \times 10^{-4}$ .

#### Determination of the hyperfine coupling constants with respect to the direction of $V_{zz}$ at <sup>35</sup>Cl

The principal axis of  $V_{zz}$  at the <sup>35</sup>Cl does not coincide with the crystallographic axes in  $\alpha$ -RuCl<sub>3</sub>. As there are also three inequivalent <sup>35</sup>Cl sites in field there is no practical way to obtain the hyperfine coupling tensor in the unit cell coordinate but it is still possible to obtain the hf couplings with respect to the axis of  $V_{zz}$  (or  $30^\circ$  off the  $c$  axis) via a direct comparison with the NMR shift  $\mathcal{K}$ . By plotting  $\mathcal{K}$  against  $\chi$  (see the inset of Fig. 2d), one obtains the hf coupling constants,  $A_{\text{hf}}^{\parallel c'} = 12.3$  kG/ $\mu_B$  and  $A_{\text{hf}}^{\perp c'} = 17.4$  kG/ $\mu_B$ , respectively, where  $\mu_B$  is the Bohr magneton. Note that, although  $\mathcal{K}_{\text{quad}}(T)$  needs to be subtracted for  $H \perp c'$ , it turns out that its correction is insignificant. If  $\mathcal{K}_{\text{quad}}(T)$  estimated above is subtracted from  $\mathcal{K}_{\perp c'}$ ,  $A_{\text{hf}}^{\perp c'}$  is only slightly reduced to 17.1 kG/ $\mu_B$ . Therefore, one can conclude that the hyperfine coupling constants are highly anisotropic. Since  $(T_1^{-1})_{\parallel H} \propto (A_{\text{hf}}^{\perp H})^2$ , to a crude approximation assuming axial symmetry, one obtains

$$\frac{(T_1^{-1})_{\parallel c'}}{(T_1^{-1})_{\perp c'}} \propto \frac{2(A_{\text{hf}}^{\perp c'})^2}{(A_{\text{hf}}^{\perp c'})^2 + (A_{\text{hf}}^{\parallel c'})^2} \sim 1.33,$$

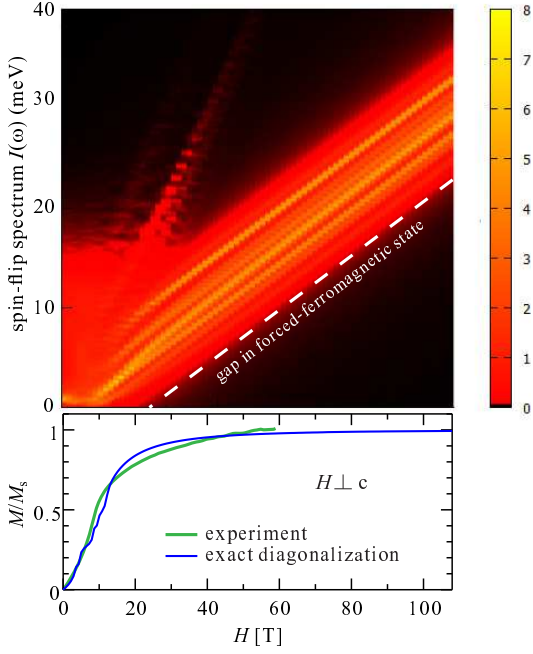


FIG. S4. Top: Spin-flip spectrum as a function of magnetic field. Bottom: comparison of experimental data and theoretical magnetization curve for  $H \perp c$  calculated for the Kitaev-Heisenberg model (Eq.2) in the parameter regime relevant for  $\alpha$ -RuCl<sub>3</sub> (see Ref. [9]). A field-forced ferromagnetic state appears for fields larger than critical field of  $H_c = 23.2$  T.

which accounts for the anisotropic  $T_1^{-1}$  at high temperatures, as shown in Fig. 2e.

### Field-induced ferromagnetic state

The basic magnetic properties of  $\alpha$ -RuCl<sub>3</sub> can be described by a spin-1/2 model on the honeycomb lattice with dominant Heisenberg and Kitaev terms. The effective Hamiltonian for a pair of Ru<sup>3+</sup> ions at sites  $i$  and  $j$  reads [9]

$$H_{ij} = J_r \tilde{\mathbf{S}}_i \cdot \tilde{\mathbf{S}}_j + K \tilde{S}_i^z \tilde{S}_j^z + \mu_B \sum_{k=i,j} \mathbf{H} \cdot \mathbf{g} \cdot \tilde{\mathbf{S}}_k \quad (2)$$

where  $\tilde{\mathbf{S}}_i$  and  $\tilde{\mathbf{S}}_j$  are 1/2-spin operators,  $J_r$  are the isotropic Heisenberg interactions between nearest- ( $r = 1$ ), second- ( $r = 2$ ), and third-neighbor ( $r = 3$ ) sites, and  $K$  is the Kitaev coupling. By fitting the magnetization calculated for a 24 site cluster with the experimental magnetization curve (Fig.S4, also see Ref. [9]) one obtains  $J_1 = 2.0$ ,  $J_2 = J_3 = 0.5$ ,  $K = -10.0$  (in unit of meV), and  $g_{\perp c} = 2.4$ . Generally, a gap opens once a ferromagnetic state is stabilized by a large magnetic field. In a typical isotropic Heisenberg model, it is known that the gap increases linearly above the saturation field  $H > H_s$ , i.e.,  $\Delta \propto H - H_s$ . However, it is a nontrivial question to find a field of the gap opening in our system (2) be-

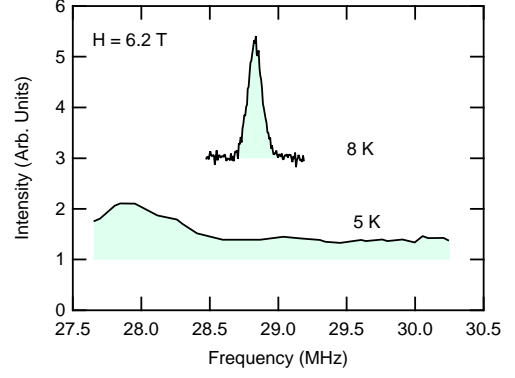


FIG. S5. Comparison of the <sup>35</sup>Cl spectrum in the PM and AFM states obtained at 6.2 T. The spectrum becomes extremely broad below  $T_N$ , evidencing the incommensurate character of the AFM ordering. The lowest frequency of the spectrum at 5 K was limited by the tuning frequency range in our experimental setup.

cause a full spin saturation  $M = M_s$  can be obtained only at  $B = \infty$ , in a strict sense, due to the presence of the Kitaev coupling. Thus, in order to estimate the gap we calculate the excitation spectrum for a spin that is flipped against the magnetic field (spin-flip spectrum), which is defined by

$$I(\omega) = \sum_{\nu} |\langle \psi_{\nu} | S_i^- | \psi_0 \rangle|^2 \delta(\omega - E_{\nu} + E_0), \quad (3)$$

where  $S_i^-$  is the spin-flip operator at site  $i$ ,  $|\psi_{\nu}\rangle$  and  $E_{\nu}$  are the  $\nu$ -th eigenstate and the eigenenergy of the system, respectively ( $\nu = 0$  corresponds to the ground state). Since the exchange fluctuations are very small in the forced ferromagnetic state, a quantitative estimation of the gap is possible even with small clusters.

The spin-flip spectrum calculated by the Lanczos exact diagonalization technique with 24-site cluster [10] is plotted in Fig.S4 (upper panel). A linear gap opening is seen in the high-field range, with the onset field  $H = 23.2$  T. This means that a forced-ferromagnetic state appears at a critical field of  $H_c = 23.2$  T. Experimentally we observe that the gap opens at a field  $\sim 10$  T, which is at least a factor of 2 lower than the forced-ferromagnetic critical field. Apart from this, the slope of the experimentally observed gap vs. field is 8.7 K/T and this is almost a factor of 3 larger than that of the forced-ferromagnetic gap, 3.1 K/T. On these grounds we can exclude that the observed gapped state corresponds to a simple field-forced ferromagnetic state.

[1] Sandilands *et al.* Scattering Continuum and Possible Fractionalized Excitations in  $\alpha$ -RuCl<sub>3</sub>. *Phys. Rev. Lett.* **114**, 147201 (2015).

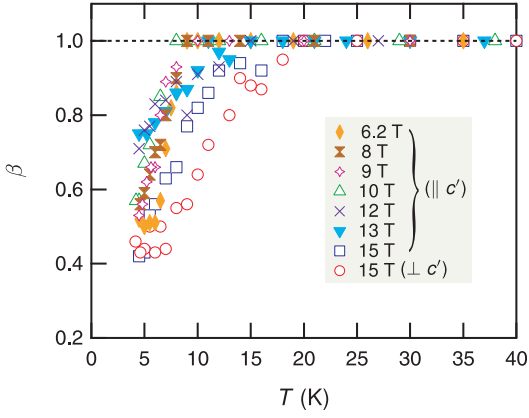


FIG. S6. The stretching exponent  $\beta$  in the spin-lattice relaxation as a function of temperature and external field.  $\beta$  rapidly decreases from unity with decreasing temperatures in the gapped spin liquid state, similar to the behavior observed in the magnetically ordered state. This indicates that short-range spin correlations persist even in the quantum disordered phase, being consistent with the plateau of  $T_1^{-1}$  deep in the spin gapped phase.

[2] Rau, J. G., Lee, E. K.-H. & Kee, H.-Y. Generic Spin

Model for the Honeycomb Iridates beyond the Kitaev Limit. *Phys. Rev. Lett.* **112**, 077204 (2014).

- [3] Majumder, M. *et al.* Anisotropic  $\text{Ru}^{3+} 4d^5$  magnetism in the  $\alpha\text{-RuCl}_3$  honeycomb system: Susceptibility, specific heat, and zero-field NMR. *Phys. Rev. B* **91**, 180401 (2015).
- [4] Sears, J. A. *et al.* Magnetic order in  $\alpha\text{-RuCl}_3$ : A honeycomb-lattice quantum magnet with strong spin-orbit coupling. *Phys. Rev. B* **91**, 144420 (2015).
- [5] Kubota, Y., Tanaka, H., Ono, T., Narumi, Y. & Kindo, K. Successive magnetic phase transitions in  $\alpha\text{-RuCl}_3$ : XY-like frustrated magnet on the honeycomb lattice. *Phys. Rev. B* **91**, 094422 (2015).
- [6] A. Banerjee, *et al.*, Proximate Kitaev quantum spin liquid behaviour in a honeycomb magnet, *Nature Mater.* **15**, 733 (2016).
- [7] Kaufmann, Elton N. & Vianden, Reiner J. The electric field gradient in noncubic metals. *Rev. Mod. Phys.* **51**, 161 (1979).
- [8] J. Nasu, M. Udagawa, & Y. Motome, Thermal fractionalization of quantum spins in a Kitaev model: Temperature-linear specific heat and coherent transport of Majorana fermions, *Phys. Rev. B* **92**, 115122 (2015).
- [9] R. Yadav, N.A. Bogdanov, V.M. Katukuri, S. Nishimoto, J. van den Brink, and L. Hozoi, *Sci. Rep.* **6**, 37925 (2016)
- [10] J. Chaloupka, G. Jackeli, and G. Khaliullin, *Phys. Rev. Lett.* **105**, 027204 (2010).